Formation of mechanism and excitonic luminescence of supercritical-fluid-synthesized ZnO nanoparticles

Brian Dusolle, Veronique Jubera, Evgeniy Ilin, Patrick Martin, Gilles Philippot, Matthew Suchomel, Bo Iversen, Samuel Marre, Cyril Aymonier

Formation Mechanism and Excitonic Luminescence of Supercritical Fluid-Synthesized ZnO Nanoparticles

Brian Dusolle[†,‡], Véronique Jubera[†], Evgeniy S. Ilin[†], Patrick Martin[#], Gilles Philippot[†], Matthew. R. Suchomel[†], Bo B. Iversen[§], Samuel Marre[†], Cyril Aymonier[†,]*

† Univ. Bordeaux, CNRS, Bordeaux INP, ICMCB, UMR 5026, F-33600 Pessac Cedex, France

‡ Univ. Bordeaux, CEA, CNRS, Bordeaux INP, IMS, UMR 5218, F-33405 Talence Cedex, France

Univ. Bordeaux, CNRS, CELIA, UMR 5107, F-33405 Talence Cedex, France

§ Center for Integrated Materials Research, Department of Chemistry and iNANO, Aarhus University, Aarhus, Denmark

*cyril.aymonier@icmcb.cnrs.fr

ABSTRACT

Extensive research on nanosized ZnO has proven that its optical properties are challenging to control, due to a number of possible defects producing various emissions in the visible range. Our group proposed a low temperature, supercritical-fluids-driven synthesis of isotropic nanosized particles which exhibit a unique and unprecedentedly pure excitonic emission, comparable to that of single crystals. The present article reports the growth mechanism at the origin of the unexpectedly pure excitonic emission, as well as a more detailed study of its optical properties at liquid helium temperatures. The ZnO phase is obtained *via* the thermal decomposition of an intermediate ZnO_2 phase. No bulk defect luminescence is detected and the synthesis route leaves a "ZnO_2-like" surface able to neutralize the formation of surface defects, which can contribute to visible emissions. The luminescence measurements were performed at liquid Helium temperature to enable the identification of excitons. The investigation of the photoluminescence properties confirms a strong excitonic emission in the UV region with no visible band, and sheds light on a phonon coupling with the E_2 high vibrational mode

INTRODUCTION

Inorganic-semiconductor-based nanostructures have become key materials for photonic applications. More stable than their organic counterparts, their optical properties are also directly related to the size, morphology, composition or defect concentration, among other parameters. In particular, zinc oxide (ZnO) is a versatile material, which has been attracting much attention as a potential candidate for light emitters, opto-chemical sensors, spin electronics, transparent electronics or piezoelectronics.[1-5] ZnO has a direct, wide bandgap (3.4 eV) leading to an ultraviolet (UV) excitonic emission, as observed in massive single crystals or thick films grown through

epitaxy processes,[6-8] and a large exciton binding energy (60 meV) leading to a reduced lasing threshold and an improved emission efficiency at room temperature.[9-12] Thus, it represents an especially interesting replacement for gallium nitride (GaN) for the design of new devices exploiting its UV luminescence. For instance, current white light emitting devices suffer from poor levels of chromaticity, which could be resolved by using highly efficient visible phosphors, as used in gas-discharge fluorescent systems, excited by a UV emitter instead. Such devices could therefore produce much richer spectra. However, UV emission is currently based on frequency doubling from infrared sources, and is consequently rather susceptible to power loss. Thus, it is essential to develop better UV emitters, and ZnO is a serious candidate.[13]

However, extensive research on nanosized ZnO has proven its optical properties challenging to control, due to a number of possible defects producing various emissions in the visible range.[14-16] The synthesis route and conditions dramatically influence the type of defects stabilized during the crystal growth,[17] thereby impacting the photoluminescence properties. Indeed, it is believed that vacancies and interstitial atoms of both zinc and oxygen can induce different deep level states in the band gap of ZnO, which both create several visible emissions and diminish the excitonic component. First of all, the atmosphere in which the materials are synthesized plays a huge role in the types of defects that are stabilized.[18] On one hand, an oxygen-rich environment promotes the formation of interstitial oxygens (O_i), a source responsible for yellow luminescence,[19,20] or zinc vacancies (V_{Zn}^{2-}, V_{Zn}^{-}), a source of both blue[20,21] and red luminescence.[22] On the other hand, a zinc-rich environment promotes the formation of interstitial zinc (Zn_i, Zn_i^{+}), a source of a purple or blue luminescence,[20,21] or oxygen vacancies (V_O, V_O^{+}); a source of a green luminescence.[20,21,23-25] Furthermore, synthesis temperature and post-synthesis heat treatments also play a role. Not only does this improve the overall luminescence intensity,[25,26]

but it can also favor certain emission peaks as some defects can only be stabilized at high temperature, making their optical footprints appear after thermal annealing.[18,21-24] For example, ZnO obtained *via* thermal oxidation of Zn films exhibits green luminescence up to 750°C, and yellow luminescence after 800°C,[23] hinting that interstitial oxygens are stabilized at high temperatures. Stacking faults in ZnO crystals also appear to influence luminescence, by creating electronic acceptor states responsible for exciton quenching[27] and a close-to-bandgap emission at 3.31 eV.[28-29] Finally, other parameters can be critical such as particles morphology,[30] dopants,[31,32] or the substrate for sputtered films.[33]

Although potentially interesting, such defect emissions can be parasitic if the UV emission is targeted. Our group proposed a low temperature, supercritical-fluids-driven synthesis of isotropic nanosized ZnO particles which exhibit a uniquely pure excitonic emission comparable to that of single crystals which generally gathered optical response from both the exciton and defects.[34,35] The first studies using a microfluidic set-up allowed the synthesis and functionalization with multiple ligands of such nanoparticles, revealing no impact of the ligands' nature on the nanoparticle growth.[34] The subsequent scaling-up of this process to millifluidics offered further control over the resulting materials, especially permitting the obtaining of different sizes and shapes according to the system's hydrodynamics.[35] In all cases, no visible fluorescence typical of zinc oxide could be observed, although the origins of such unique properties were not extensively studied. The present article reports the growth mechanism at the origin of the unexpectedly pure excitonic emission, as well as a more detailed study of its optical properties at liquid helium temperature.

EXPERIMENTAL

Synthesis

The set-up used for the synthesis has already been described elsewhere.[34] Briefly, it consists of two pumps, a reactor and a back pressure regulator. The reactor is made of two coaxial tubes: the internal, 20-centimeter-long tube (ID = 1 mm, OD = 1/16") is placed inside of the external, one-meter-long tube (ID= 2.1 mm, OD = 1/8"), which is itself placed inside a furnace. A solution containing zinc acetylacetonate monohydrate ($Zn(acac)_2 \cdot H_2O$) and hydrogen peroxide (35 wt% H_2O_2 in water solution) in absolute ethanol is injected with the first pump into the internal tube, while absolute ethanol is injected with the second pump in the external tube, thus creating a concentric flow focusing configuration, which is pressurized at 25 MPa using the back pressure regulator, and brought to 250 °C by the furnace. A series of four samples have been synthesized using four different residence times (6 s, 10 s, 30 s and 40 s). The final dispersions of ZnO nanoparticles ($ZnO\text{-}NP_{Ø}$) in ethanol were collected downstream of the back-pressure regulator. ZnO nanopowders were recovered by centrifugation at 9000 rpm or by simple Büchner filtration, washed several times in absolute ethanol at room temperature and kept in ethanol. All chemicals were used as received from Sigma-Aldrich.

CHARACTERIZATION

X-ray diffraction analyses

Ex situ X-ray powder diffraction measurements (XRD) were recorded with a PANalitical X'Pert Pro powder diffractometer in the Bragg-Brentano geometry using a Cu Kα source

($\lambda \approx 1.5406$ Å) at room temperature over the angular 2θ range 8°-80° with a step of 0.02°. The samples were prepared by depositing a ZnO suspension on a silicon substrate.

In situ temperature-dependent diffraction data were collected at the high-energy powder diffraction beamline P02.1 of the Petra III synchrotron using a wavelength of 0.206 Å (60 keV). Two-dimensional data were measured by a PerkinElmer amorphous silicon detector. The setup used for the measurements was described in details elsewhere.[36,37] For this experiment, a fused silica capillary was filled with the precursor solution and pressurized using a high pressure pump. The capillary was later heated with a jet of hot air. After reaching equilibrium conditions for each temperature step, 60 frames (1 second each) of data were averaged, azimuthally integrated, and converted into one-dimensional 2θ versus intensity data using the FIT2D software.[38] Reference background patterns measured on capillaries containing only solvent at equivalent pressure and temperature conditions were subtracted from each *in situ* data set using the CMPR software.[39] Pawley profile refinements of the 2θ versus intensity data powder diffraction data were performed using the TOPAS software package.[40] Values were refined for the sample lattice parameters, Chebyshev background polynomial, and Lorentzian crystallite size using the integral breadth (LVol-IB) model. Instrument profile parameters were obtained from a profile fit of LaB_6 data measured with an identical beamline configuration.

High resolution transmission electron microscopy (HRTEM)

HRTEM observations were performed using a JEOL 2200 FS equipped with a field gun emission, operating at 200 kV and with a point resolution of 0.23 nm. HRTEM micrographs and size distribution diagrams were calculated for about 100 nanoparticles.

Optical characterizations

The photoluminescence (PL) properties were analysed using a SPEX FL212 Jobin-Yvon spectrofluorimeter in a front face configuration. The excitation spectra were corrected for the variation of the incident flux and the emission spectra were corrected for the transmission of the monochromator and the response of the photomultiplier. The equipment consists of a 450 W xenon lamp, an excitation double monochromator (1200 lines/mm UV gratings 250 nm blaze), an emission double monochromator (1200 lines/mm UV gratings 330 nm blaze) and a thermoelectrically cooled photomultiplier tube. The wavelength positions of the excitation and emission monochromators were adjusted by using a specific mercury calibration lamp. Slits apertures, increments and acquisition times were adjusted for optimized signal-to-noise ratio and resolution. The resolution was equal to 0.2 meV at 367.4 nm.

All samples were prepared from suspensions of nanoparticles in ethanol that were drop-cast onto a quartz plate and dried for several hours at 80°C. Low temperature PL measurements were carried out on samples synthesized with 40 s residence time using an Oxford cryostat, as well as a pumping system to ensure the circulation of helium gas, thus allowing measurements down to 4 K. The temperature was monitored using a thermal probe in direct contact with the sample holder.

Raman diffusion

Raman spectra were measured using a Thermo scientific DXR micro-Raman spectrometer under a 523 nm laser excitation (power of 10 mW) at room temperature. Samples were prepared by depositing a small amount of powder on a glass plate.

RESULTS AND DISCUSSION

Particle growth mechanism

This section highlights the understanding of the formation mechanism of ZnO nanoparticles in the supercritical reactor in order to explain their unique optical properties. Our hypothesis is that the ZnO phase is obtained via the thermal decomposition of an intermediate ZnO_2 phase, leaving a "ZnO_2-like" surface able to neutralize the formation of surface defects usually responsible for visible emissions. This theory is supported by previous reports of ZnO_2 formation from ZnO exposition to H_2O_2.[41] Here, it is implied that H_2O_2 allows the formation of ZnO_2 which is quickly thermally converted into ZnO. A series of *ex situ* and *in situ* characterizations have been performed in order to confirm this mechanism.

X-ray diffraction patterns and Raman spectra for each sample obtained at 6, 10, 30 and 40s are shown in Figure 1A and 1B, respectively. Rietveld refinements were also performed to better estimate the average crystallite size (A.C.S) and lattice parameters for each sample. The results of our refinements are presented in Table 1, and plots of the final refinement cycles can be seen in Figure S1.

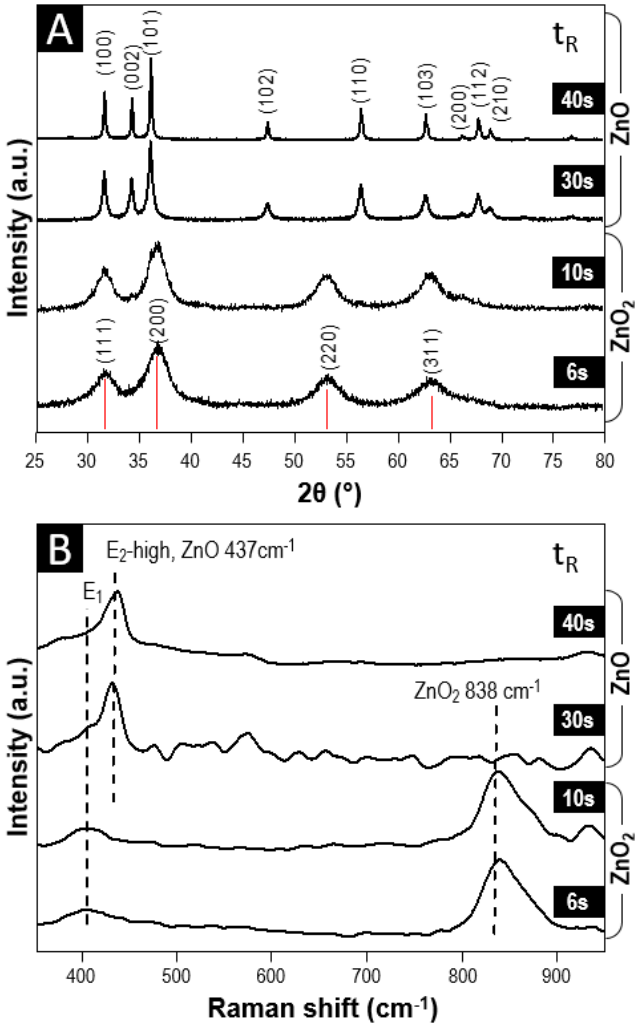

Figure 1. Evolution of (A) X-Ray diffraction patterns and (B) Raman spectra of Zn-based materials as a function of residence time (t_R).

Table 1. Values of average crystallite size (A.C.S.) and lattice parameters as obtained from Rietveld refinements of materials prepared at several residence times. The space groups used to perform the refinements where Pa-3 and $P6_3mc$ for ZnO_2 and ZnO, respectively.

Residence time t_r (s)	6	10	30	40
Crystalline phase	ZnO_2	ZnO_2	ZnO	ZnO

A.C.S. (nm)	2.3 ± 0.1	2.9 ± 0.1	12.9 ± 0.1	30.8 ± 0.1
Lattice parameters (Å)	a=4.864(1)	a=4.867(1)	a= 3.250(1) c= 5.208(1)	a= 3.250(1) c= 5.207(1)
R-factor	2.52	1.26	5.54	6.90
χ^2	2.21	0.329	0.746	0.344

A clear dependence of the crystalline structure as a function of the residence time can be observed. On one hand, the samples synthesized at lower residence times (6 s and 10 s) exhibit patterns consistent with a zinc peroxide cubic phase with a lattice parameter of 4.864 Å (ZnO_2, JCPDS card No. 13-0311).[42-46] On the other hand, the samples synthesized at higher residence times (30 s and 40 s) exhibit patterns consistent with a zinc oxide hexagonal phase with lattice parameters of a=3.250 Å and c=5.207 Å (Wurtzite structure, JCPDS No. 00-036-1451). These results are consistent with Raman analyses displayed on Figure 1B, which show a clear transition from ZnO_2 to ZnO between 10 s and 30 s residence time. Crystallite sizes also appear to be increasing with residence time, ranging from 2.3 nm at 6 s to 30.8 nm at 40 s.

In order to confirm the presence of ZnO into ZnO_2 nanoparticles, XPS measurements were performed on the samples obtained with 6 s and 40 s residence times. Figure 2 shows XPS survey spectra of the sample obtained with 6 s residence time at low and high energy regions.

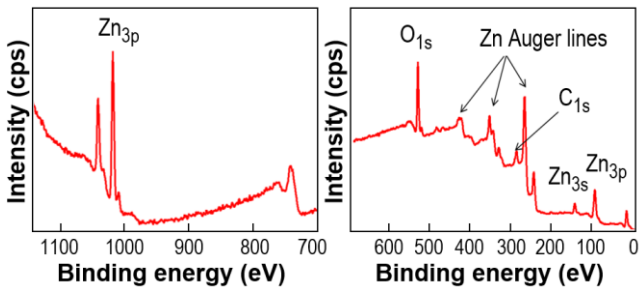

Figure 2. XPS survey spectra at low and high energy regions of ZnO_2 sample obtained with 6 s residence time.

The survey spectra of this ZnO_2 sample have several lines, which can be attributed to $Zn_{3s,3p}$, O_{1s}, C_{1s} atoms. Additionally, these spectra exhibit Auger lines of Zn atoms such as ZnML1 and ZnML2 peaks. The spectra of the ZnO NPØ sample obtained with a residence time of 40 s (not shown here) have similar shapes to that of the 6 s residency ZnO_2 sample. High-resolution XPS spectra were measured on Zn_{3p} (Figure 3C and D) and O_{1s} (Figure 3A and B) atoms for both samples in order to get information concerning the presence of ZnO phase in ZnO_2 nanoparticles. Measurements on Zn_{3p} proved a Zn^{2+} oxidation states for all Zn atoms in both samples. Figure 3A shows the XPS spectrum of the sample obtained with 6 s residence time. This spectrum can be fitted with three functions corresponding to binding energies at 530.6 eV, 532.2 eV and 533.2 eV.

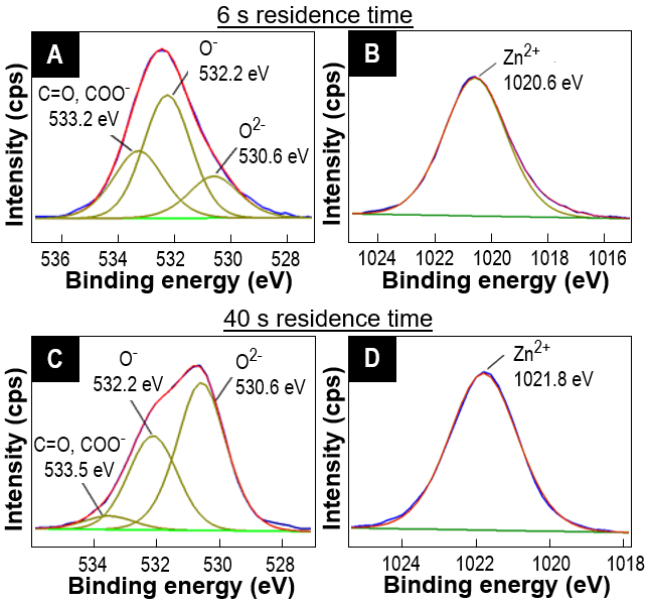

Figure 3 High resolution XPS spectra measured on O1s (A and C) and Zn_{3p} (B and D) atoms for the samples obtained with 6 s (A end B) and 40 s (C and D) residence times.

According to Dupin *et al.* the binding energy of O_{1s} atom in the range of 527-530 eV is characteristic of O^{2-} ions in metal oxides.[47] The binding energy in the range of 530.6-531.1 eV is characteristic of oxygen species integrated in the material O_2^{2-}. The binding energy in the range of 531.1-532 eV is due to low coordinated oxygen species, which may be described as "O^-" ions. Khallaf *et al.* have also reported O_{1s} XPS spectra for ZnO_2, where the observed binding energy for ZnO_2 is equal to 532 eV, while annealed ZnO_2 sample exhibits XPS line at 530 eV corresponding to ZnO.[48] Thereby, the binding energies of O_{1s} atom in the sample obtained with a residence time of 6 s at 530.6 eV, 532.2 eV and 533.2 eV could be attributed to O^{2-}, O^- from O_2^{2-} ions and oxygen originating from the organic functions as C=O, COO^-, respectively.

A high resolution O_{1s} XPS spectrum of the sample obtained for the 40 s residence time sample is presented in Figure 3C. As in the previous case, this spectrum can be fitted with three functions with corresponding binding energies of 530.6 eV, 532.2 eV and 533.5 eV, and these binding energies can also be attributed to O^{2-}, O^- and C=O, COO^-, respectively. The quantification based on XPS spectra resulted in, for the 6s residence time ZnO_2 sample, 9.02 at% O^{2-} and 24.53 at% O^-, and for the 40s residence time ZnO sample, 22.67 at% O^{2-} and 14.09 at% O^-. It should be noted that all information gathered by XPS relates to the near surface region of the investigated material.

According to XRD, Raman and XPS characterizations, ZnO Wurtzite phase is mainly obtained in experiments at longer residence times (30 s and 40 s), while a ZnO_2 cubic phase is observed for the shorter residence times (6 s and 10 s). These experimental results are consistent with a hypothesis that ZnO nanoparticles could be formed through the intermediate ZnO_2 phase formed by $Zn(acac)_2{\cdot}H_2O$ transformation in the presence of H_2O_2 in a supercritical ethanol/water mixture. Moreover, it is known that ZnO_2 is a compound with a quite low decomposition temperature equal

to 200°C.[48-51] Thereby, ZnO_2 intermediate nanoparticles could be thermally decomposed to ZnO in the supercritical reactor used in this work (250 °C, 25 MPa).

In situ powder diffraction measurements were performed in order to highlight the conversion of a ZnO_2 intermediate phase into the final ZnO nanoparticles. The precursor solution was first pressurized at 25 MPa, then the temperature was increased step by step in order to slow the reaction down and be able to see this phase transition. Indeed, at a fixed temperature of 250°C, the reaction is too fast (a few seconds) to measure diffraction patterns with good statistics. Figure 4c shows that the ZnO_2 intermediate phase starts to be formed at room temperature and is stable up to 150°C. Then, when the temperature is further increased, this intermediate phase starts to disappear, and at 200 °C the ZnO phase appears.

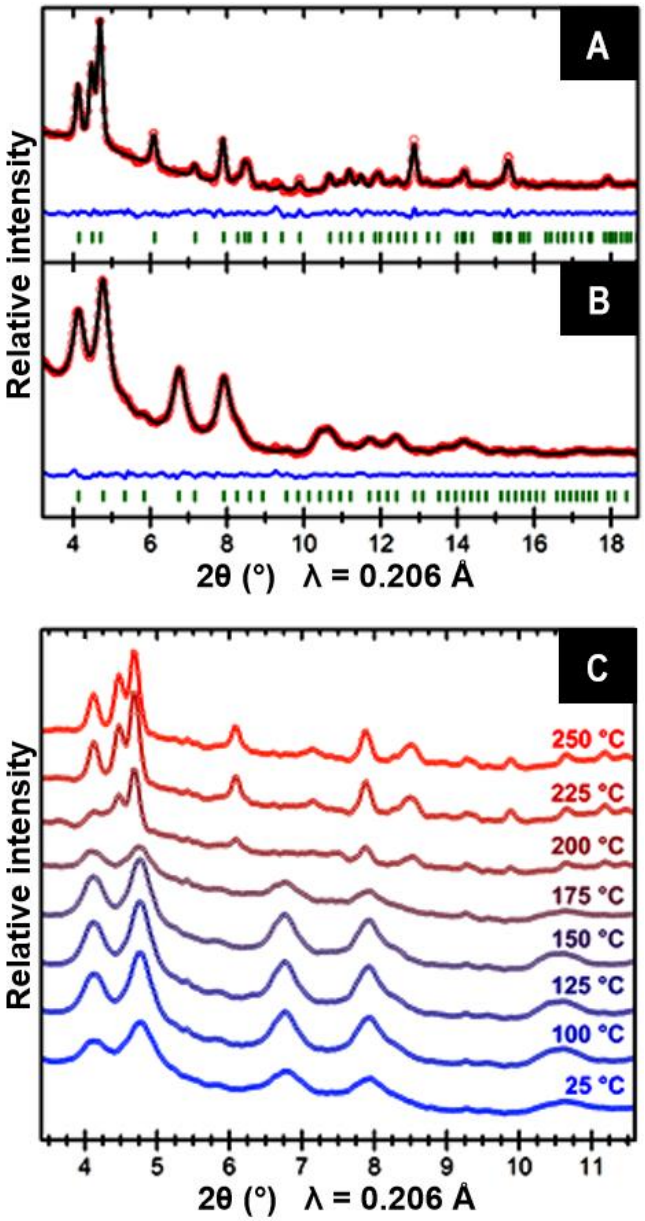

Figure 4 Pawley profile refinements of *in situ* powder diffraction data measured at (A) 225°C and (B) 125°C, and (C) *in situ* powder diffraction patterns for the series of increasing temperature, showing a clear structural transition at approximately 175°C.

Data at 225°C (Figure 4a) are fit using the $P6_3mc$ space group (n 186) of Wurtzite-type ZnO with refined lattice parameters of a=3.291(1) Å and c=5.257(2) Å. This is consistent with reported

ambient temperature lattice values for bulk ZnO of a≈3.25 Å and c≈5.206 Å (ICSD 162843, Kim *et al.* 2008[52]). A crystallite size around 20 nm is estimated from the refined Lorentzian size parameter.

Data at 125 °C (Figure 4b) are fit using the cubic *Pa*-3 space group (n 205) of pyrite-type ZnO_2 with a refined lattice parameter of a=4.947(1) Å. This is consistent with the reported ambient temperature lattice value for bulk ZnO_2 of a≈4.87 Å (ICSD 60763, Pušelj *et al.* 1985[53]). A crystallite size arround 2.5 nm is estimated from the refined Lorentzian size parameter.

The values of crystallite sizes obtained *in situ* at both temperatures are consistent with the range deduced from *ex situ* measurements. This evolution supports the idea that ZnO_2 is an intermediate seed that will then be reorganized into ZnO with an increase of temperature. Note that the refined lattice values are consistently larger than the cited bulk literature values, as expected due to thermal expansion of the unit cell at the elevated measurement temperatures and possible atomic relaxation effects due to the nanoscale particle size. An excellent fit to the experimental data is observed at both temperatures, with R_{wp}=1.6 % and 1.5 % for 225 °C and 125 °C, respectively.

Results of HRTEM analyses are displayed in Figure 5. Micrographs obtained at high magnification and corresponding size histograms are shown for each of the four samples previously described. Every sample exhibits rather spherical nanoparticles of sizes seemingly increasing with residence time (3.4 ± 0.6 nm after 6 s, 4.6 ± 0.8 nm after 10 s, 12.8 ± 3.5 nm after 30 s and 12.9 ± 3 nm after 40 s). However, no significant evolution can be observed between the last two samples, indicating that the Zn precursor is completely decomposed after 30 s in the reactor. Moreover, TEM micrographs reveal a good crystallinity which is specific to materials obtained in supercritical conditions.[54] There is a good agreement between A.C.S determined by XRD and nanoparticle size determined by TEM, except for the sample obtained at 40s. A reason

for this observation could be the settling of the particles inside the reactor. Indeed, in order to reach longer residence times, the flowrate (and therefore the flow velocity) needs to be reduced. Hence, the inertial forces acting on the NPs are weaker, which could result in NPs deposition inside the reactor. For 6, 10 and 30 s residence time, ZnO nanoparticles are recovered continuously with no material being extracted during the reactor cleaning step. This is not the case for the sample recovered at 40 s residence time, thus supporting our hypothesis. HRTEM and all the other characterizations have been performed on the nanoparticles recovered continuously, except XRD performed on both kinds of nanoparticles (recovered continuously and after cleaning, meaning with the highest residence time in the reactor and the biggest size) to get enough material for the analysis.

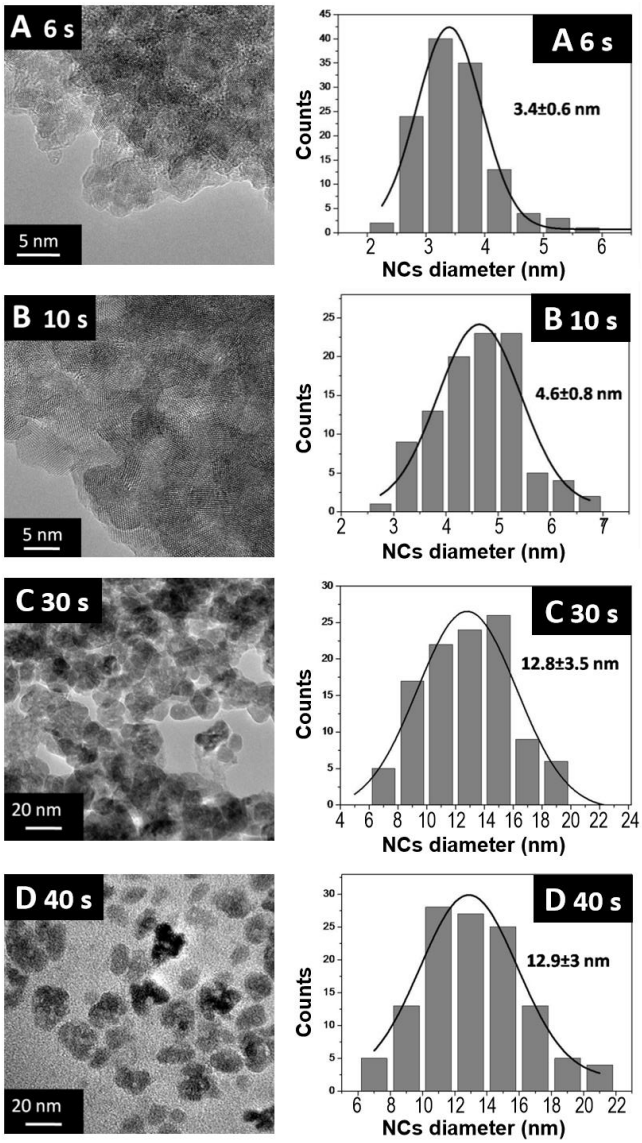

Figure 5 HRTEM micrographs of ZnO_2 nanoparticles and corresponding histograms for the samples obtained with a residence time of (A) 6 s, (B) 10 s, (C) 30 s and (D) 40 s.

As a conclusion, all *ex situ* and *in situ* analyses revealed that the ZnO nanoparticles synthesized with the supercritical route originate from the thermal decomposition of a ZnO_2 phase, leading to a peculiar "ZnO_2-like" surface, as depicted in Figure 6. The surface is believed to be the reason for the observed purely excitonic emission (see below), as further heat-treatment leads to the

appearance of a visible emission feature (Figure S2),[34,35] which also underlines how important H_2O_2 is to prevent the stabilization of oxygen vacancies both in the core material and on its surface (Figure S3).

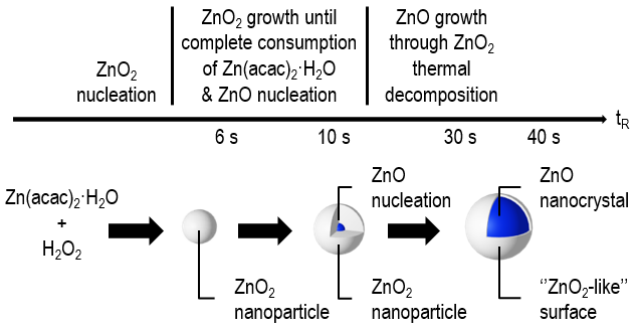

Figure 6 Diagram of ZnO nanoparticles growth through thermally induced ZnO_2 decomposition in the supercritical reactor.

Description of the excitonic emission

A freshly-prepared suspension of nanoparticles ($NP_{Øfresh}$) and another sample prepared 12 months prior and stored in ethanol ($NP_Ø$) were deposited on a quartz plate to be deeply optically characterized. A single crystal provided by Tokyo Denpa Co., Ltd was also characterized under the same conditions to provide a reference of the spectral distribution obtained with our particular set-up. The luminescence measurements were performed at liquid Helium temperature to enable the identification of excitons.

Emission spectra were obtained under excitation at a 325 nm wavelength. No difference could be observed between $NP_Ø$ and $NP_{Øfresh}$, proving the good stability of the particles over time when stored in ethanol. Figure 7 illustrates results for the $NP_Ø$ and the single crystal. A well-structured

ultraviolet emission is present in both samples, however the single crystal also shows traces of a visible band whereas the corresponding range is flat for the $NP_{Ø}$ (Figure 7A, Figure S4).

Figure 7B shows the band-edge region of the $NP_{Ø}$ emission spectrum between 3.25 eV and 3.4 eV where three narrow peaks can be distinguished. In order of decreasing intensity: the first line is detected at 3.375 eV (367.6 nm); the second one is detected at 3.32 eV, which is 55 meV (456 cm^{-1}) lower than the first one ; and the last, smaller one is detected at 3.34 eV, in between the two more intense ones.

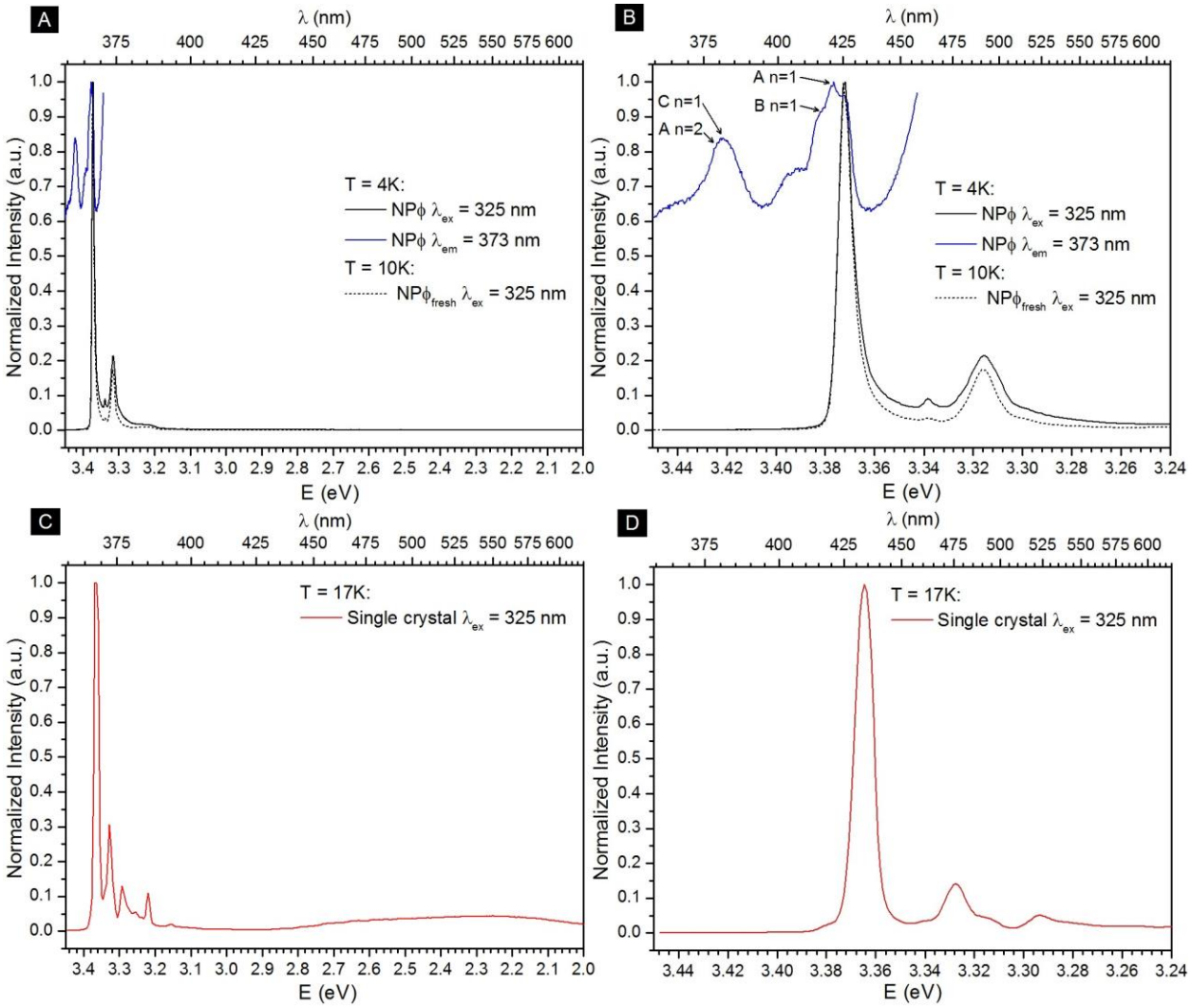

Figure 7 Luminescence spectra of ZnO materials performed at liquid Helium temperature.

(A) Excitation and emission spectra and (B) zoom in the UV range for the NPØ. (C) Emission spectrum and (D) zoom in the UV range for the single crystal.

The excitation spectrum of the NPØ was collected by fixing the emission wavelength at 373 nm. The excitation spectrum is constituted of several groups of lines. The classical nomenclature for the threefold degenerated sub-valence bands, which are labelled as A, B and C from top to bottom, respectively in the ZnO Wurtzite type semiconductor, has been chosen to name the different lines observed. The exciton having a hydrogen-like set of energy levels, and these last ones can be expressed as follow:

$$E_n = E_{gap} - \frac{EI}{n^2}$$

n being the main quantum number, and EI the exciton ionization energy.

Table 2 lists the peak positions and their potential attribution. Data observed on single crystals and reported by D.G. Thomas and W.Y. Liang *et al.* are indicated for comparison.[6,55] Some additional calculated positions are given assuming the $1/n^2$ relation for the successive quantum states.[55-58]

Table 2. Position of the intrinsic exciton state at 4.2 K. (*calculated) (**not well discriminated)

Exciton nature	Quantum state	NPØ particles		Single crystal[6,55]	
		Peak position (eV)	E_i-$E_{An=1}$ (eV)	Peak position (eV)[53]	Peak position (eV)[6]
A	n=1	3.375	---	3.3768	3.3781
	n=2	3.421	0.046*	3.4225	3.4282
	n=3	3.429*	0.054*	---	3.4375*
	n=∞	3.436*	0.061*	3.4358*	3.4449*

B	n=1	3.382	0.007*	3.3830	3.3856
	n=2	---	---	3.4275	3.4324
C	n=1	3.42**	0.045*	3.4215	3.4264

Considering the experimental data listed in Table 2, the exciton ionization energy (EI), has been calculated as follows, giving a value of 0.061 eV.

$$EI = \frac{4}{3}(E_2 - E_1)$$

with E_1=3.375 eV* and E_2=3.421 eV* (*experimental value illustrated in Figure 7).

Surprisingly for such small particles, these energies associated with peak positions detected on the excitation curve are in excellent agreement with those observed in low temperature polarized transmission spectra performed on single crystals and described in references.[6,59] This definitely confirms the good crystallinity of the nanoparticles.

A comparison between the excitation and emission curves shows a good matching between the highest energy emission line located at 3.375 eV and the lowest energy absorption line (Figure 7, A and B for nanoparticles, C and D for the provided single crystals). Emission lines ranging from 3.375-3.38 eV are fully described in the literature. These peaks are attributed to the reverse absorption phenomenon *i.e.* the direct radiative electron-hole recombination called free excitonic recombination (FX line). Concerning the nanoparticles, within these FX radiative emissions, one can distinguish several types of free excitonic recombination depending on the energy levels involved in the transition. (labelled as FX_A, FX_B, FX_C[60]…) The energy difference between FX_A and FX_B is generally comprised between 7 meV and 10 meV, FX_A being the line at lower energy,[6-8,61] which is consistent with the energy difference observed on the excitation curve. However, many reports[62-64] on ZnO nanowires, films and nanorods show that FX associated emission appears

at temperature higher than 10 K after the depopulation of traps which gives lines peaking between 3.358 eV-3.367 eV.[59] This lower energy emission originates from excitons bound with ionized or neutral donors (D^+, D^0) or neutral acceptors (A^0) thus forming D^+X, D^0X and A^0X centers. Such an emission was reported as intense narrow emission peak at low temperature observed in ZnO single crystals, films and nanowires.[57,65-70]

In addition to FX and the bound excitons, some authors report the existence of lines between 3.32 eV and 3.34 eV.[63,70,71] These emissions are called two-electron satellite (TES) transitions. TES is originated from the radiative recombination of a neutral donor bound exciton (D^0X) with a neutral donor and excited free exciton. Therefore, TES emission could only be observed in the presence of neutral donor bound exciton emission.[56]

Low temperature luminescence measurements have been carried out on various ZnO nanostructures (Table S1). To our knowledge, the smallest structures to exhibit FX emission at low temperature are nanorod-like structures with sizes down to 50 nm. Moreover, spectral features linked to bounded excitons are described as groups of thin lines in the 3.365-3.368 eV range, *i.e.* at lower energies than the most observed intense line, however no such contributions can be observed in Figure 7B.

The presence of emission lines at energies classically associated with free exciton recombination is rather unexpected for nanostructures such as $NP_{Ø}$. However, two hypotheses can be formulated: either (*i*) a quantum confinement effect due to small particle sizes generates a shift of bound exciton emissions towards higher energies, or (*ii*) the specific synthetic route avoids the stabilization of intrinsic point defects leading to unhindered free excitonic emissions. In the former case, according to V. A. Fonoberov *et al.* and their study on ZnO nanoparticles ranging from 1.6 nm to 6 nm,[72,73] UV emissions could arise from the recombination of either confined excitons

(observed in particles with radii lower than 2 nm) or surface-bound ionized-acceptor-exciton complexes (leading to a 100-200 meV Stokes shift), depending on fabrication process and surface quality.

However, no Stokes shift can be observed between the excitation and emission graphs on Figure 7, and the average crystallite size of $NP_{Ø}$ has been estimated at 13 nm, a much higher value than the Wurtzite ZnO Bohr radius (2.34 nm[74,75]), which invalidates our first hypothesis. Therefore, the latter hypothesis is retained, meaning the most intense line can be attributed to FX_A free-excitonic recombinations. Our singular route, leading to small sizes and good crystallinity, can thus be held accountable for the absence of local defect centers which would otherwise trap the electron-hole pairs generated under UV excitation and which are required for the observation of bound excitons in the expected 3.35-3.37 eV energy region.

The second broader line detected at lower energy than the FX_A line is peaking at 3.32 eV (energy difference being equal to 56 eV/452 cm^{-1}). In order to understand the nature of the emission lines, Raman spectroscopy measurements were performed (Figure 1B) and the Raman diffusion graph of the $NP_{Ø}$ was superimposed onto the emission spectra which was shifted for the main peak to be positioned at 0 cm^{-1} (Figure 8).

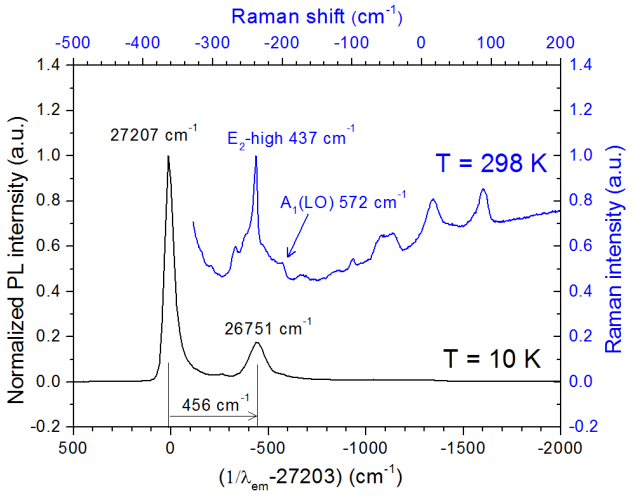

Figure 8 Superimposition of the emission spectrum measured at 10 K (λ_{ex} = 325 nm) and the room temperature Raman spectrum of ZnO nanoparticles.

Besides confirming the ZnO phase, a good agreement is observed between the vibrational energy of the E_2 high non polar mode at 436 cm^{-1} and the second line peaking roughly 456 cm^{-1} below the most intense line. The investigations of the optical phonons and the emission properties of ZnO have been provided by a number of groups.[76-82] The Wurtzite-type ZnO unit cell presents 12 phonon modes, 9 of which are optical. The zone-centered optical phonons can be classified according to the following representation: $\Gamma_{opt}=A_1+E_1+2E_2+2B_1$. The A_1 and E_1 optical modes are polar and both Raman and IR active, the two E_2 modes are nonpolar and Raman active only, and the B_1 optical mode is inactive. Raman shifts are equal to 437 cm^{-1}, 583 cm^{-1} and 574 cm^{-1} for optical modes E_2, E_1(LO) and A_1(LO), respectively.[76-78] Temperature dependence of Raman scattering of E_2-high, A_1(LO) and E_1(LO) modes have been reported by Cuscó *et al.*[79] The authors describe the evolution of intensity and the frequency shift to higher values as temperature decreases from 750 K to 80 K. The E_2 high mode expected at higher frequencies for lower temperatures can justify the small shift observed in Figure 8 between the Raman and the emission spectra shown at

10 K. At low temperature, the emitted state in the emission spectra of ZnO single crystals, nanorods and films are mostly attributed to the coupling of excitons with A_1(LO) phonons and E_1 optical Raman modes as shown in Figure 8 and Table S1, the energy difference being equal to about 75 meV (585 cm^{-1}). Jeong *et al.*[81] have more recently reported the broadening of linewidth of acceptor bound exciton line (A^0X) located at 3.3581 eV at 13 K resulting from a coupling with the E_2-high vibration phonon mode. Considering the calculated energy difference observed between the most intense lines and the possibility to observe a coupling between the FX_A excitons and the E_2 high nonpolar mode, the line located at 3.32 eV (373.8 nm) should be attributed to a vibronic transition.

Moreover, additional Raman spectroscopy analyses confirm the presence of two different structures according to residence time (Figure 1B). Raman spectra of the samples synthesized at higher residence times (30 s and 40 s) display two obvious vibrational bands at 415 cm^{-1} and 437 cm^{-1} corresponding to E_1 polar and E_2-high nonpolar optical Raman mode of ZnO Wurtzite structure.[77] However, the spectra of the samples obtained at lower residence times (6 s and 10 s) both show a strong and broad band located at 838 cm^{-1}, which was observed before in ZnO_2 nanoparticles,[49-51,83-85] and was attributed by Uekawa *et al.* to the stretching vibrations of the O-O bond of the peroxo ion (O_2^{2-}),[50] thus corroborating the XRD data. Yet, they also show a weak and broad band between 395 cm^{-1} and 419 cm^{-1}, which could be attributed to the E_1 polar mode of ZnO Wurtzite structure, although the respective XRD patterns show no evidence of a ZnO phase in those samples. This result can be explained by a ZnO phase inside the ZnO_2 particles at a concentration below 5 wt%, corresponding to the XRD sensitivity threshold, thus providing further proof of the previously stated hypothesis regarding the thermal decomposition of ZnO_2 into ZnO.

Finally, a small peak is also visible at 3.340 eV between the two more intense lines (Figure 7B). This peak observed at 4 K, although close to the TES energy region, cannot be attributed to such emission as no bound exciton lines or additional visible emission corresponding to donor or acceptor defects was observed on the emission spectra, as mentioned previously. In addition, S. Inguva *et al.* also reported a novel emission at 3.331 eV, proposing its origin to be linked to an electron-hole recombination at structural defects associated with the boundary interface region of the crystalline-ZnO@amorphous-ZnO core/shell nanorods grown on Si (100) wafers.[86] Thonke *et al*. pointed lines in this energy range due to basal plane stacking faults (BSF) of the Wurtzite type structure,[86-88] corresponding to the thinnest segment of ZnO Blende phase inserted in the Wurtzite matrix. They identified the peak at 3.329 eV as the recombination of the confined indirect exciton in the BSFs.

Considering that the NPØ sample comes from the decomposition of ZnO_2 cubic nuclei,[89] this last hypothesis seems to be a better explanation for the small contribution observed around 3.34 eV (371 nm). The final attribution of NPØ emission peaks is indicated in Table 3.

Table 3. Final attribution of the peaks observed in ZnO nanoparticles synthesized *via* the supercritical fluids route.

	FX_C	**FX_B**	**FX_A**	**D^0X**	**A^0X → BSF**	**TES → FX_A - E_2 high**	**LO-DX**	**LO-FX**
NPØ (This work)	-	3.382	3.375	-	3.34	3.32 (FX_A - E_2 high)	-	-

Conclusions

In summary, an array of characterizations was performed in order to deduce the structure and supercritical-fluids-induced growth mechanism leading to ZnO nanoparticles with a pure excitonic luminescence. *Ex situ* analyses on samples synthesized at different residence times and *in situ* analyses on growing particles confirmed the formation of ZnO via thermal decomposition of a prior ZnO_2 phase, thus leaving a peculiar "ZnO_2-like" surface at the origin the optical properties. These photoluminescence properties were investigated in detail using low temperature measurements, confirming a strong excitonic emission in the UV region with no visible band, and shedding light on a phonon coupling with the E_2 high mode.

ASSOCIATED CONTENT

Supporting Information. The following file is available free of charge.

Supplementary characterization of samples synthesized at different residence times and further literature study of ZnO optical properties (PDF)

AUTHOR INFORMATION

Corresponding Author

cyril.aymonier@icmcb.cnrs.fr

Author Contributions

The manuscript was written through contributions of all authors. All authors have given approval to the final version of the manuscript. B. Dusolle: Contribution to the original draft and Editing ; V. Jubera: Investigation, Writing original draft, Revision and Editing ; E. Ilin: Investigation, Writing original draft ; P. Martin: Investigation of the optical properties ; G. Philippot:

Investigation of the in situ experiments and Editing ; M.R. Suchomel: Processing and analysis of in situ diffraction data and Editing ; B.B. Iversen: Access to beam time for in situ investigations and Editing ; S. Marre: Revision and Editing ; C. Aymonier: Investigation, Supervision, Writing original draft, Revision and Editing.

ACKNOWLEDGMENT

The authors thank the CNRS and the Nouvelle Aquitaine region. This study was carried out with financial support from the French State, managed by the French National Research Agency (ANR) in the frame of a non-thematic program (ANR-2010-BLANC-0820) and in the frame of "the Investments for the future" Program IDEX Bordeaux – LAPHIA (ANR-10-IDEX-03-02).

The Villum Foundation is thanked for support. We gratefully acknowledge DESY (Hamburg, Germany), a member of the Helmholz Association HGF, for granting beamtime at PETRA-III.

The authors also thank Sonia Buffière, Eric Lebraud for providing SEM pictures and powder XRD diffraction patterns and Alexandre Fargues for the optical setup adaptation.

We also acknowledge the support from the LIGHT S&T Graduate Program (PIA3 Investment for the Future Program, ANR-17-EURE-0027).

REFERENCES

(1) Nomura, K.; Ohta, H.; Ueda, K.; Kamiya, T.; Hirano, M.; Hosono, H. Thin-Film Transistor Fabricated In Single-Crystalline Transparent Oxide Semiconductor. *Science* **2003**, *300* (5623), 1269–1272. DOI: 10.1126/science.1083212.

(2) Könenkamp, R.; Word, R. C.; Schlegel, C. Vertical Nanowire Light-emitting Diode. *Appl. Phys. Lett.* **2004**, *85* (24), 6004–6006. DOI: 10.1063/1.1836873.

(3) Wagh, M.; Patil, L.; Seth, T.; Amalnerkar, D. Surface Cupricated SnO_2-ZnO Thick Films As A H_2S Gas Sensor. *Mater. Chem. Phys.* **2004**, *84* (2-3), 228–233. DOI: 10.1016/s0254-0584(03)00232-3.

(4) Pearton, S. J.; Heo, W. H.; Ivill, M.; Norton, D. P.; Steiner, T. Dilute Magnetic Semiconducting Oxides. *Semicond Sci. Technol.* **2004**, *19* (10), R59–R74. DOI: 10.1088/0268-1242/19/10/r01.

(5) Ushio, Y.; Miyayama, M.; Yanagida, H. Effects Of Interface States On Gas-sensing Properties Of A CuO/ZnO Thin-film Heterojunction. *Sens. Actuators B Chem.* **1994**, *17* (3), 221–226. DOI: 10.1016/0925-4005(93)00878-3.

(6) Liang, W. Y.; Yoffe, A. D. Transmission Spectra Of ZnO Single Crystals. *Phys. Rev. Lett.* **1968**, *20* (2), 59–62. DOI: 10.1103/physrevlett.20.59.

(7) Makino, T.; Chia, C. H.; Tuan, N. T.; Segawa, Y.; Kawasaki, M.; Ohtomo, A.; Tamura, K.; Koinuma, H. Exciton Spectra Of ZnO Epitaxial Layers On Lattice-matched Substrates Grown With Laser-molecular-beam Epitaxy. *Appl. Phys. Lett.* **2000**, *76* (24), 3549–3551. DOI: 10.1063/1.126703.

(8) Jung, S. W.; Park, W. I.; Cheong, H. D.; Yi, G.-C.; Jang, H. M.; Hong, S.; Joo, T. Time-resolved And Time-integrated Photoluminescence In ZnO Epilayers Grown On Al_2O_3(0001) By Metalorganic Vapor Phase Epitaxy. *Appl. Phys. Lett.* **2002**, *80* (11), 1924–1926. DOI: 10.1063/1.1461051.

(9) Yang, P.; Yan, H.; Mao, S.; Russo, R.; Johnson, J.; Saykally, R.; Morris, N.; Pham, J.; He, R.; Choi, H.-J. Controlled Growth Of ZnO Nanowires And Their Optical Properties. *Adv. Funct.*

Mater. **2002**, *12* (5), 323. DOI: 10.1002/1616-3028(20020517)12:5<323::aid-adfm323>3.0.co;2-g.

(10) Qin, F. F.; Xu, C. X.; Zhu, Q. X.; Lu, J. F.; Chen, F.; You, D. T.; Zhu, Z.; Manohari, A. G. Optical Performance Improvement In Hydrothermal ZnO/graphene Structures For Ultraviolet Lasing. *J. Mater. Chem. C* **2018**, *6* (13), 3240–3244. DOI: 10.1039/c7tc05880b.

(11) Hong, J. T.; Park, J.-Y.; Lee, S.; Ahn, Y. H. UV-induced Terahertz Wave Modulation In Free-standing ZnO Nanowire Films. *Opt. Mater. Express* **2016**, *6* (12), 3751. DOI: 10.1364/ome.6.003751.

(12) Zhu, G. Investigation Of The Mode Structures Of Multiphoton Induced Ultraviolet Laser In A ZnO Microrod. *Journal of Nanotechnology* **2017**, *2017*, 1–5. DOI: 10.1155/2017/3931210.

(13) Fiedler, S.; Lee Cheong Lem, L. O.; Ton-That, C.; Schleuning, M.; Hoffmann A.; Phillips M. R. Correlative Study Of Enhanced Excitonic Emission In Zno Coated With Al Nanoparticles Using Electron And Laser Excitation, Scientific Reports **2020**, 10, 2553. DOI: s41598-020-59326-3.

(14) Dijken, A. van; Meulenkamp, E. A.; Vanmaekelbergh, D.; Meijerink, A. The Kinetics Of The Radiative And Nonradiative Processes In Nanocrystalline ZnO Particles Upon Photoexcitation. *The Journal of Physical Chemistry B* **2000**, *104* (8), 1715–1723. DOI: 10.1021/jp993327z.

(15) Kahn, M. L.; Glaria, A.; Pages, C.; Monge, M.; Macary, L. S.; Maisonnat, A.; Chaudret, B. Organometallic Chemistry: An Alternative Approach Towards Metal Oxide Nanoparticles. *J. Mater. Chem.* **2009**, *19* (24), 4044. DOI: 10.1039/b818935h.

(16) Kahn, M. L.; Monge, M.; Collière, V.; Senocq, F.; Maisonnat, A.; Chaudret, B. Size- And Shape-Control Of Crystalline Zinc Oxide Nanoparticles: A New Organometallic Synthetic Method. *Adv. Funct. Mater.* **2005**, *15* (3), 458–468. DOI: 10.1002/adfm.200400113.

(17) Jensen, K. M. Ø.; Christensen, M.; Juhas, P.; Tyrsted, C.; Bøjesen, E. D.; Lock, N.; Billinge, S. J. L.; Iversen, B. B. Revealing The Mechanisms Behind SnO2 Nanoparticle Formation And Growth During Hydrothermal Synthesis: An In Situ Total Scattering Study. *Journal of the American Chemical Society* **2012**, *134* (15), 6785–6792. DOI: 10.1021/ja300978f.

(18) Murkute, P.; Ghadi, H.; Sreedhara, S.; Chakrabarti, S. Detailed Investigation Of Photoluminescence, Structural, And Elemental Properties Of ZnO Thin Films Under Various Annealing Ambient. *Superlattices Microstruct.* **2019**, *136*, 106310. DOI: 10.1016/j.spmi.2019.106310.

(19) Banerjee, D.; Kar, A. K. Effect Of Hydroxide Ion Concentration On The Evolution Of Nanostructures And Structure Correlated Luminescence Of ZnO Nanopowders. *Opt. Mater.* **2019**, *89*, 430–440. DOI: 10.1016/j.optmat.2019.01.048.

(20) Camarda, P.; Vaccaro, L.; Sciortino, A.; Messina, F.; Buscarino, G.; Agnello, S.; Gelardi, F. M.; Popescu, R.; Schneider, R.; Gerthsen, D.; Cannas, M. Synthesis Of Multi-color Luminescent ZnO Nanoparticles By Ultra-short Pulsed Laser Ablation. *Appl. Surf. Sci.* **2020**, *506*, 144954. DOI: 10.1016/j.apsusc.2019.144954.

(21) Mondal, P. Effect Of Oxygen Vacancy Induced Defect On The Optical Emission And Excitonic Lifetime Of Intrinsic ZnO. *Opt. Mater.* **2019**, *98*, 109476. DOI: 10.1016/j.optmat.2019.109476.

(22) Anantachaisilp, S.; Smith, S. M.; Ton-That, C.; Pornsuwan, S.; Moon, A. R.; Nenstiel, C.; Hoffmann, A.; Phillips, M. R. Nature Of Red Luminescence In Oxygen Treated Hydrothermally Grown Zinc Oxide Nanorods. *J. Lumin.* **2015**, *168*, 20–25. DOI: 10.1016/j.jlumin.2015.07.025.

(23) Wang, Y. .; Lau, S. .; Zhang, X. .; Lee, H. .; Yu, S. .; Tay, B. .; Hng, H. . Evolution Of Visible Luminescence In ZnO By Thermal Oxidation Of Zinc Films. *Chem. Phys. Lett.* **2003**, *375* (1-2), 113–118. DOI: 10.1016/s0009-2614(03)00842-x.

(24) Camarda, P.; Messina, F.; Vaccaro, L.; Agnello, S.; Buscarino, G.; Schneider, R.; Popescu, R.; Gerthsen, D.; Lorenzi, R.; Gelardi, F. M.; Cannas, M. Luminescence Mechanisms Of Defective ZnO Nanoparticles. *Phys. Chem. Chem. Phys.* **2016**, *18* (24), 16237–16244. DOI: 10.1039/c6cp01513a.

(25) Nkosi, S. S.; Kortidis, I.; Motaung, D. E.; Kroon, R. E.; Leshabane, N.; Tshilongo, J.; Ndwandwe, O. M. The Effect Of Stabilized ZnO Nanostructures Green Luminescence Towards LPG Sensing Capabilities. *Mater. Chem. Phys.* **2020**, *242*, 122452. DOI: 10.1016/j.matchemphys.2019.122452.

(26) Chen, W.; Yao, C.; Gan, J.; Jiang, K.; Hu, Z.; Lin, J.; Xu, N.; Sun, J.; Wu, J. ZnO Colloids And ZnO Nanoparticles Synthesized By Pulsed Laser Ablation Of Zinc Powders In Water. *Mater. Sci. Semicond. Process.* **2020**, *109*, 104918. DOI: 10.1016/j.mssp.2020.104918.

(27) Sieber, B.; Addad, A.; Szunerits, S.; Boukherroub, R. Stacking Faults-Induced Quenching Of The UV Luminescence In ZnO. *The Journal of Physical Chemistry Letters* **2010**, *1* (20), 3033–3038. DOI: 10.1021/jz101267t.

(28) Schirra, M.; Schneider, R.; Reiser, A.; Prinz, G. M.; Feneberg, M.; Biskupek, J.; Kaiser, U.; Krill, C. E.; Thonke, K.; Sauer, R. Stacking Fault Related 3.31-eV Luminescence At 130-meV Acceptors In Zinc Oxide. *Phys. Rev. B* **2008**, *77* (12), 125215. DOI: 10.1103/physrevb.77.125215.

(29) Schirra, M.; Schneider, R.; Reiser, A.; Prinz, G. M.; Feneberg, M.; Biskupek, J.; Kaiser, U.; Krill, C. E.; Sauer, R.; Thonke, K. Acceptor-related Luminescence At 3.314 eV In Zinc Oxide Confined To Crystallographic Line Defects. *Phys. B: Condens. Matter* **2007**, *401-402*, 362–365. DOI: 10.1016/j.physb.2007.08.188.

(30) Rackauskas, S.; Klimova, O.; Jiang, H.; Nikitenko, A.; Chernenko, K. A.; Shandakov, S. D.; Kauppinen, E. I.; Tolochko, O. V.; Nasibulin, A. G. A Novel Method For Continuous Synthesis Of ZnO Tetrapods. *The Journal of Physical Chemistry C* **2015**, *119* (28), 16366–16373. DOI: 10.1021/acs.jpcc.5b03702.

(31) Govindaraj, R.; Govindan, R.; Geetha, M.; Anbarasan, P. M. Structural, Morphological And Luminescence Studies On Pristine And La Doped Zinc Oxide (ZnO) Nanoparticles. *Optik* **2015**, *126* (17), 1555–1558. DOI: 10.1016/j.ijleo.2015.04.043.

(32) Mosquera, E. Influence Of Bi Doping On The Luminescence Of ZnO Phosphors. *Optik* **2020**, *218*, 165102. DOI: 10.1016/j.ijleo.2020.165102.

(33) Mendil, D.; Challali, F.; Touam, T.; Chelouche, A.; Souici, A. H.; Ouhenia, S.; Djouadi, D. Influence Of Growth Time And Substrate Type On The Microstructure And Luminescence Properties Of ZnO Thin Films Deposited By RF Sputtering. *J. Lumin.* **2019**, *215*, 116631. DOI: 10.1016/j.jlumin.2019.116631.

(34) Ilin, E. S.; Marre, S.; Jubera, V.; Aymonier, C. Continuous Supercritical Synthesis Of High Quality UV-emitting ZnO Nanocrystals For Optochemical Applications. *J. Mater. Chem. C* **2013**, *1* (33), 5058. DOI: 10.1039/c3tc30737a.

(35) Roig, Y.; Marre, S.; Cardinal, T.; Aymonier, C. Synthesis Of Exciton Luminescent ZnO Nanocrystals Using Continuous Supercritical Microfluidics. *Angew. Chem.* **2011**, *123* (50), 12277–12280. DOI: 10.1002/ange.201106201.

(36) Becker, J.; Bremholm, M.; Tyrsted, C.; Pauw, B.; Jensen, K. M. Ø.; Eltzholt, J.; Christensen, M.; Iversen, B. B. Experimental Setup For In Situ X-ray SAXS/WAXS/PDF Studies Of The Formation And Growth Of Nanoparticles In Near- And Supercritical Fluids. *J. Appl. Crystallogr.* **2010**, *43* (4), 729–736. DOI: 10.1107/s0021889810014688.

(37) Philippot, G.; Jensen, K. M. Ø.; Christensen, M.; Elissalde, C.; Maglione, M.; Iversen, B. B.; Aymonier, C. Coupling In Situ Synchrotron Radiation With Ex Situ Spectroscopy Characterizations To Study The Formation Of $Ba_{1-x}Sr_xTiO_3$ Nanoparticles In Supercritical Fluids. *The Journal of Supercritical Fluids* **2014**, *87*, 111–117. DOI: 10.1016/j.supflu.2013.12.009.

(38) Hammersley, A. P.; Svensson, S. O.; Hanfland, M.; Fitch, A. N.; Hausermann, D. Two-dimensional Detector Software: From Real Detector To Idealised Image Or Two-theta Scan. *High Pressure Research* **1996**, *14* (4-6), 235–248. DOI: 10.1080/08957959608201408.

(39) Toby, B. H. CMPR - A Powder Diffraction Toolkit. *J. Appl. Crystallogr.* **2005**, *38* (6), 1040–1041. DOI: 10.1107/s0021889805030232.

(40) Coelho, A. A.; Evans, J.; Evans, I.; Kern, A.; Parsons, S. The TOPAS Symbolic Computation System. *Powder Diffr*. **2011**, *26* (S1), S22–S25. DOI: 10.1154/1.3661087.

(41) Lingampalli, S. R.; Dileep, K.; Datta, R.; Gautam, U. K. Tuning The Oxygen Release Temperature Of Metal Peroxides Over A Wide Range By Formation Of Solid Solutions. *Chem. Mater.* **2014**, *26* (8), 2720-2725. DOI: 10.1021/cm500622u.

(42) Escobedo-Morales, A.; Esparza, R.; Garcıa-Ruiz, A.; Aguilar, A.; Rubio-Rosas, E.; Pérez, R. Structural And Vibrational Properties Of Hydrothermally Grown ZnO_2 Nanoparticles. *J. Cryst. Growth* **2011**, *316* (1), 37–41. DOI: 10.1016/j.jcrysgro.2010.12.057.

(43) Vannerberg, N. G. The Infrared Spectra Of Some Peroxide Hydrates. *Arkiv Kemi* **1959**, *14* (11), 107–113.

(44) Cheng, S.; Yan, D.; Chen, J. T.; Zhuo, R. F.; Feng, J. J.; Li, H. J.; Feng, H. T.; Yan, P. X. Soft-Template Synthesis And Characterization Of ZnO_2 And ZnO Hollow Spheres. *The Journal of Physical Chemistry C* **2009**, *113* (31), 13630–13635. DOI: 10.1021/jp9036028.

(45) Pemartin, K.; Solans, C.; Vidal-Lopez, G.; Sanchez-Dominguez, M. Synthesis Of ZnO And ZnO_2 Nanoparticles By The Oil-in-water Microemulsion Reaction Method. *Chem. Lett.* **2012**, *41* (10), 1032–1034. DOI: 10.1246/cl.2012.1032.

(46) Rosenthal-Toib, L.; Zohar, K.; Alagem, M.; Tsur, Y. Synthesis Of Stabilized Nanoparticles Of Zinc Peroxide. *Chem. Eng. J.* **2008**, *136* (2-3), 425–429. DOI: 10.1016/j.cej.2007.07.071.

(47) Dupin, J.-C.; Gonbeau, D.; Vinatier, P.; Levasseur, A. Systematic XPS Studies Of Metal Oxides, Hydroxides And Peroxides. *Phys. Chem. Chem. Phys.* **2000**, *2* (6), 1319–1324. DOI: 10.1039/a908800h.

(48) Khallaf, H.; Chai, G.; Lupan, O.; Heinrich, H.; Park, S.; Schulte, A.; Chow, L. Investigation Of Chemical Bath Deposition Of ZnO Thin Films Using Six Different Complexing Agents. *J. Phys. D: Appl. Phys.* **2009**, *42* (13), 135304. DOI: 10.1088/0022-3727/42/13/135304.

(49) Kim, K.-A.; Cha, J.-R.; Gong, M.-S.; Kim, J.-G. Preparation Of ZnO_2 Nanoparticles Using Organometallic Zinc(II) Isobutylcarbamate In Organic Solvent. *Bull. Korean Chem. Soc.* **2014**, *35* (2), 431–435.

(50) Uekawa, N.; Mochizuki, N.; Kajiwara, J.; Mori, F.; Wu, Y. J.; Kakegawa, K. Nonstoichiometric Properties Of Zinc Oxide Nanoparticles Prepared By Decomposition Of Zinc Peroxide. *Phys. Chem. Chem. Phys.* **2003**, *5* (5), 929–934. DOI: 10.1039/b210990e.

(51) Sun, M.; Hao, W.; Wang, C.; Wang, T. A Simple And Green Approach For Preparation Of ZnO_2 And ZnO Under Sunlight Irradiation. *Chem. Phys. Lett.* **2007**, *443* (4-6), 342–346. DOI: 10.1016/j.cplett.2007.06.098.

(52) Kim, Y.-I.; Cadars, S.; Shayib, R.; Proffen, T.; Feigerle, C. S.; Chmelka, B. F.; Seshadri, R. Local Structures Of Polar Wurtzites Zn1-xMgxO Studied By Raman And 67Zn/25Mg NMR Spectroscopies And By Total Neutron Scattering. *Phys. Rev. B* **2008**, *78* (19), 195205. DOI: 10.1103/physrevb.78.195205.

(53) Pušelj, M.; Ban, Z.; Morvaj, J. On The Peroxydes Of Zinc And Cadmium. *Croat. Chem. Acta* **1985**, *58* (3), 283–288.

(54) Aymonier, C.; Philippot, G.; Erriguible, A.; Marre, S. Playing With Chemistry In Supercritical Solvents And The Associated Technologies For Advanced Materials By Design. *The Journal of Supercritical Fluids* **2018**, *134*, 184–196. DOI: 10.1016/j.supflu.2017.12.021.

(55) Thomas, D. G. The Exciton Spectrum Of Zinc Oxide. *J. Phys. Chem. Solids* **1960**, *15* (1-2), 86–96. DOI: 10.1016/0022-3697(60)90104-9.

(56) Hopfdeld, J. J. Fine Structure In The Optical Absorption Edge Of Anisotropic Crystals. *J. Phys. Chem. Solids* **1960**, *15* (1-2), 97–107. DOI: 10.1016/0022-3697(60)90105-0.

(57) Reynolds, D. C.; Litton, C. W.; Collins, T. C. Zeeman Effects In The Edge Emission And Absorption Of ZnO. *Phys. Rev.* **1965**, *140* (5A), A1726–A1734. DOI: 10.1103/physrev.140.a1726.

(58) Klingshirn, C. F. *Semiconductor Optics*. Springer Berlin Heidelberg, 2012. DOI: 10.1007/978-3-642-28362-8.

(59) Meyer, B. K.; Alves, H.; Hofmann, D. M.; Kriegseis, W.; Forster, D.; Bertram, F.; Christen, J.; Hoffmann, A.; Straßburg, M.; Dworzak, M.; Haboeck, U.; Rodina, A. V. Bound Exciton And Donor–acceptor Pair Recombinations In ZnO. *Phys. Status Solidi B* **2004**, *241* (2), 231–260. DOI: 10.1002/pssb.200301962.

(60) Klingshirn, C. ZnO: Material, Physics And Applications. *ChemPhysChem* **2007**, *8* (6), 782–803. DOI: 10.1002/cphc.200700002.

(61) Ahn, C. H.; Mohanta, S. K.; Lee, N. E.; Cho, H. K. Enhanced Exciton-phonon Interactions In Photoluminescence Of ZnO Nanopencils. *Appl. Phys. Lett.* **2009**, *94* (26), 261904. DOI: 10.1063/1.3159829.

(62) Khranovskyy, V.; Glushenkov, A. M.; Chen, Y.; Khalid, A.; Zhang, H.; Hultman, L.; Monemar, B.; Yakimova, R. Crystal Phase Engineered Quantum Wells In ZnO Nanowires. *Nanotechnology* **2013**, *24* (21), 215202. DOI: 10.1088/0957-4484/24/21/215202.

(63) Borysiewicz, M. A.; Wzorek, M.; Wojciechowski, T.; Wojtowicz, T.; Kaminska, E.; Piotrowska, A. Photoluminescence Of Nanocoral ZnO Films. *J. Lumin.* **2014**, *147*, 367–371. DOI: 10.1016/j.jlumin.2013.11.076.

(64) Zhang, R.; Yin, P.-G.; Wang, N.; Guo, L. Photoluminescence And Raman Scattering Of ZnO Nanorods. *Solid State Sci.* **2009**, *11* (4), 865–869. DOI: 10.1016/j.solidstatesciences.2008.10.016.

(65) Reynolds, D. C.; Look, D. C.; Jogai, B.; Litton, C. W.; Collins, T. C.; Harsch, W.; Cantwell, G. Neutral-donor-bound-exciton Complexes In ZnO Crystals. *Phys. Rev. B* **1998**, *57* (19), 12151–12155. DOI: 10.1103/physrevb.57.12151.

(66) Hamby, D. W.; Lucca, D. A.; Klopfstein, M. J.; Cantwell, G. Temperature Dependent Exciton Photoluminescence Of Bulk ZnO. *J. Appl. Phys.* **2003**, *93* (6), 3214–3217. DOI: 10.1063/1.1545157.

(67) Park, W. I.; Yi, G.-C. Photoluminescent Properties Of ZnO Thin Films Grown On SiO_2/Si(100) By Metal-organic Chemical Vapor Deposition. *J. Electron. Mater.* **2001**, *30* (10), L32–L35. DOI: 10.1007/s11664-001-0127-7.

(68) Park, W. I.; Yi, G.-C.; Jang, H. M. Metalorganic Vapor-phase Epitaxial Growth And Photoluminescent Properties Of $Zn_{1-x}Mg_xO$ ($0 \leq x \leq 0.49$) Thin Films. *Appl. Phys. Lett.* **2001**, *79* (13), 2022–2024. DOI: 10.1063/1.1405811.

(69) Li, L. M.; Li, C. C.; Zhang, J.; Du, Z. F.; Zou, B. S.; Yu, H. C.; Wang, Y. G.; Wang, T. H. Bandgap Narrowing And Ethanol Sensing Properties Of In-doped ZnO Nanowires. *Nanotechnology* **2007**, *18* (22), 225504. DOI: 10.1088/0957-4484/18/22/225504.

(70) Teke, A.; Özgür, Ü.; Dogan, S.; Gu, X.; Morkoç, H.; Nemeth, B.; Nause, J.; Everitt, H. O. Excitonic Fine Structure And Recombination Dynamics In Single-crystalline ZnO. *Phys. Rev. B* **2004**, *70* (19), 195207. DOI: 10.1103/physrevb.70.195207.

(71) Wang, X. H.; Xu, S. J. Two-electron-satellite Transition Of Donor Bound Exciton In ZnO: Radiative Auger Effect. *Appl. Phys. Lett.* **2013**, *102* (18), 181909. DOI: 10.1063/1.4804619.

(72) Fonoberov, V. A.; Balandin, A. A. Origin Of Ultraviolet Photoluminescence In ZnO Quantum Dots: Confined Excitons Versus Surface-bound Impurity Exciton Complexes. *Appl. Phys. Lett.* **2004**, *85* (24), 5971–5973. DOI: 10.1063/1.1835992.

(73) Fonoberov, V. A.; Balandin, A. A. Radiative Lifetime Of Excitons In ZnO Nanocrystals: The Dead-layer Effect. *Phys. Rev. B* **2004**, *70* (19), 195410. DOI: 10.1103/physrevb.70.195410.

(74) Gu, Y.; Kuskovsky, I. L.; Yin, M.; O'Brien, S.; Neumark, G. F. Quantum Confinement In ZnO Nanorods. *Appl. Phys. Lett.* **2004**, *85* (17), 3833–3835. DOI: 10.1063/1.1811797.

(75) Senger, R. T.; Bajaj, K. K. Optical Properties Of Confined Polaronic Excitons In Spherical Ionic Quantum Dots. *Phys. Rev. B* **2003**, *68* (4), 045313. DOI: 10.1103/physrevb.68.045313.

(76) Damen, T. C.; Porto, S. P. S.; Tell, B. Raman Effect In Zinc Oxide. *Phys. Rev.* **1966**, *142* (2), 570–574. DOI: 10.1103/physrev.142.570.

(77) Arguello, C. A.; Rousseau, D. L.; Porto, S. P. S. First-Order Raman Effect In Wurtzite-Type Crystals. *Phys. Rev.* **1969**, *181* (3), 1351–1363. DOI: 10.1103/physrev.181.1351.

(78) Calleja, J. M.; Cardona, M. Resonant Raman Scattering In ZnO. *Phys. Rev. B* **1977**, *16* (8), 3753–3761. DOI: 10.1103/physrevb.16.3753.

(79) Cuscó, R.; Alarcón-Lladó, E.; Ibáñez, J.; Artús, L.; Jiménez, J.; Wang, B.; Callahan, M. J. Temperature Dependence Of Raman Scattering In ZnO. *Phys. Rev. B* **2007**, *75* (16), 165202. DOI: 10.1103/physrevb.75.165202.

(80) Hauschild, R.; Priller, H.; Decker, M.; Brückner, J.; Kalt, H.; Klingshirn, C. Temperature Dependent Band Gap And Homogeneous Line Broadening Of The Exciton Emission In ZnO. *Phys. Status Solidi C* **2006**, *3* (4), 976–979. DOI: 10.1002/pssc.200564643.

(81) Jeong, T. S.; Yu, J. H.; Mo, H. S.; Kim, T. S.; Lim, K. Y.; Youn, C. J.; Hong, K. J. Characteristic Properties Of Raman Scattering And Photoluminescence On ZnO Crystals Doped Through Phosphorous-ion Implantation. *J. Appl. Phys.* **2014**, *115* (5), 053521. DOI: 10.1063/1.4864714.

(82) Park, Y. S.; Litton, C. W.; Collins, T. C.; Reynolds, D. C. Exciton Spectrum Of ZnO. *Phys. Rev.* **1966**, *143* (2), 512–519. DOI: 10.1103/physrev.143.512.

(83) Yang, L. Y.; Feng, G. P.; Wang, T. X. Green Synthesis Of ZnO_2 Nanoparticles From Hydrozincite And Hydrogen Peroxide At Room Temperature. *Mater. Lett.* **2010**, *64* (14), 1647–1649. DOI: 10.1016/j.matlet.2010.04.022.

(84) Feng, G.; Yang, L.; Wang, T.; Zhang, J.; Lou, T. Hydrothermal Preparation Of Nanocrystalline ZnO_2. *Particuology* **2012**, *10* (3), 388–391. DOI: 10.1016/j.partic.2011.06.010.

(85) Bai, H.; Liu, X. Green Hydrothermal Synthesis And Photoluminescence Property Of ZnO_2 Nanoparticles. *Mater. Lett.* **2010**, *64* (3), 341–343. DOI: 10.1016/j.matlet.2009.11.008.

(86) Inguva, S.; Marka, S. K.; Vijayaraghavan, R. K.; McGlynn, E.; Srikanth, V. V. S. S.; Mosnier, J.-P. Crystalline ZnO/Amorphous ZnO Core/Shell Nanorods: Self-Organized Growth,

Structure, And Novel Luminescence. *The Journal of Physical Chemistry C* **2015**, *119* (9), 4848–4855. DOI: 10.1021/jp511783c.

(87) Thonke, K.; Schirra, M.; Schneider, R.; Reiser, A.; Prinz, G. M.; Feneberg, M.; Biskupek, J.; Kaiser, U.; Sauer, R. The Role Of Stacking Faults And Their Associated 0.13 eV Acceptor State In Doped And Undoped ZnO Layers And Nanostructures. *Microelectron. J.* **2009**, *40* (2), 210–214. DOI: 10.1016/j.mejo.2008.07.031.

(88) Thonke, K.; Schirra, M.; Schneider, R.; Reiser, A.; Prinz, G. M.; Feneberg, M.; Sauer, R.; Biskupek, J.; Kaiser, U. The Role Of Stacking Faults And Their Associated 0.13 eV Acceptor State In Doped And Undoped ZnO Layers And Nanostructures. *Phys. Status Solidi B* **2010**, *247* (6), 1464–1468. DOI: 10.1002/pssb.200983273.

(89) Ilin, E. Study Of The Synthesis Mechanisms And Optical Properties Of ZnO Nanomaterials Obtained By Supercritical Fluids Route. Ph.D. Thesis, Université de Bordeaux, Bordeaux, France, 2017.

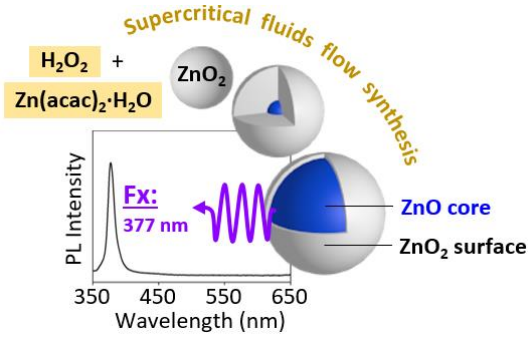

For table of content only